



Gradient-based wind farm layout optimization with inclusion and exclusion zones

Javier Criado Risco^{1,a}, Rafael Valotta Rodrigues^{1,b}, Mikkel Friis-Møller¹, Julian Quick¹,
Mads Mølgaard Pedersen¹, and Pierre-Elouan Réthoré¹

¹Wind Energy and Power Systems, Technical University Of Denmark,
Frederiksborgvej 399, 4000 Roskilde, Denmark

^anow at: Ørsted, Nesa Allé 1, 2820 Gentofte, Denmark

^bnow at: Electrical and Computer Engineering Department, University of Massachusetts Boston,
100 Morrissey Blvd, Boston, MA 02125, United States of America

Correspondence: Javier Criado Risco (j.criado.risco@gmail.com)

Received: 19 January 2023 – Discussion started: 21 February 2023

Revised: 18 November 2023 – Accepted: 9 January 2024 – Published: 14 March 2024

Abstract. Wind farm layout optimization is usually subjected to boundary constraints of irregular shapes. The analytical expressions of these shapes are rarely available, and, consequently, it can be challenging to include them in the mathematical formulation of the problem. This paper presents a new methodology to integrate multiple disconnected and irregular domain boundaries in wind farm layout optimization problems. The method relies on the analytical gradients of the distances between wind turbine locations and boundaries, which are represented by polygons. This parameterized representation of boundary locations allows for a continuous optimization formulation. A limitation of the method, if combined with gradient-based solvers, is that wind turbines are placed within the nearest polygons when the optimization is started in order to satisfy the boundary constraints; thus the allocation of wind turbines per polygon is highly dependent on the initial guess. To overcome this and improve the quality of the solutions, two independent strategies are proposed. A case study is presented to demonstrate the applicability of the method and the proposed strategies. In this study, a wind farm layout is optimized in order to maximize the annual energy production (AEP) in a non-uniform wind resource site. The problem is constrained by the minimum distance between wind turbines and five irregular polygon boundaries, defined as inclusion zones. Initial guesses are used to instantiate the optimization problem, which is solved following three independent approaches: (1) a baseline approach that uses a gradient-based solver; (2) approach 1 combined with the relaxation of the boundaries, which allows for a better design space exploration; and (3) the application of a heuristic algorithm, “smart-start”, prior to the gradient-based optimization, improving the allocation of wind turbines within the inclusion polygons based on the potential wind resource and the available area. The results show that the relaxation of boundaries combined with a gradient-based solver achieves on average +10.2 % of AEP over the baseline, whilst the smart-start algorithm, combined with a gradient-based solver, finds on average +20.5 % of AEP with respect to the baseline and +9.4 % of AEP with respect to the relaxation strategy.

1 Introduction

Wind farm layout design is usually subjected to geometric constraints, which can be dictated by seabed conditions, water depth, or local maritime routes in offshore projects, or by land ownership, presence of other infrastructure, or existence of humid areas and waterways in onshore projects (Dalla Longa et al., 2018). An ideal configuration would consist of a single regular and convex polygon within which all the wind turbines are placed. However, developers usually have to deal with multiple complex and non-connected shapes that complicate the farm design phase.

When irregular, disconnected, and non-convex-shaped polygons are involved, the wind farm layout optimization framework becomes challenging, as it is not straightforward to include analytical expressions of these areas in the problem formulation. Despite a lot of research work having been done in the field of wind farm layout optimization, less attention has been given to the implementation of complex-shaped boundaries. Mittal and Mitra (2019) pointed out the “gap towards the development of methods that lead to high-quality solutions while considering constraints such as forbidden areas”. Reddy (2021) discusses the lack of “a robust method for modeling irregular, non-convex, and disconnected domains”.

Much of the prior work in optimizing wind farms with irregular boundaries has focused on discrete parameterization of the domain and polygon representation to handle the constraints. Perez-Moreno et al. (2018) dealt with the preliminary design of the turbine layout, electrical collection system, and support structures following first a sequential approach and then a multidisciplinary approach. For these purposes, they divided the design space into squares to enable the optimization with a particle swarm optimization (PSO) algorithm. González et al. (2017) compared two metaheuristic optimization algorithms (genetic algorithm and particle swarm optimization) to solve the layout optimization problem considering realistic constraints for the concession zone and the maximum area. For their work, they discretized their domain, as an analytical expression for these constraints was not available. Chen and MacDonald (2014) involved land ownership participation rates in the wind farm layout optimization problem. They split their domain into cells in order to account for the different land owners. Tao et al. (2021) show an optimization example with two restriction zones (an ellipse and a regular convex polygon), with straightforward analytical expressions due to the simple shapes. The whole domain was later discretized before the optimization was run, excluding the grid points that belonged to the forbidden zones. Mittal and Mitra (2019) solved a multi-objective wind farm optimization problem with restricted areas within their domain by discretizing the area into a uniform set of grids. Shakoor et al. (2016) approached the problem using definite point selection, considering an irregular polygon exclusion zone within a discretized domain. Sorkhabi et al. (2018) present a continuous genetic algorithm

optimization approach, only discretizing the domain when handling exclusion zone constraints.

A disadvantage of discretizing the domain is that there is a trade-off between the quality of the solution and the resolution of the grid. A thinner grid will lead to a higher-quality solution, whilst it will also increase the computational effort significantly (Mittal and Mitra, 2019; Masoudi and Baneshi, 2022). Other strategies to integrate different boundaries include dividing the domain into polygons and/or applying penalty functions. The disadvantage of penalty methods is that they can result in turbines being moved in and out of exclusion zones or regions of nearby turbines, leading to longer optimization runs. A penalty method would require some sort of smoothing, which the Lagrange multiplier provides, avoiding these oscillations. Sorkhabi et al. (2016) considered restricted areas defined by means of convex polygon representation. The polygon vertices are joined with the wind turbine positions, forming triangles. If the area of the triangles is equal to the area of the polygon, the turbine is located inside the polygon. Then, the constraints are integrated within the optimization framework by means of penalty functions. Feng et al. (2018) solved the annual energy production (AEP) maximization problem in complex terrain with convex-shaped polygon boundary constraints. Their method, however, cannot handle irregular non-convex boundaries. Hou et al. (2016) developed a layout optimization using particle swarm optimization (PSO) considering two restriction zones in a construction sea area, corresponding to an oil well and a gas pipe/marine traffic lane. The implementation associated with the restriction areas used a penalty function, which required a penalty factor value assumption. Optimized solutions will, though, be sensitive to the choice of the penalty factor parameter. Similarly, the work done by Afanasyeva et al. (2018) considered exclusion zones through the use of a penalty function. Wang et al. (2015) present a genetic algorithm optimization approach for wind farm layouts where exclusion zones are filtered as a pre-processing step. Another approach was described in Reddy (2021), where a solution for modeling irregular, disconnected, complex, and non-convex polygons was proposed. This methodology aims at simplifying complex domain boundaries and land constraints with the support vector domain description (SVDD) technique. The SVDD is used to convert the regions into a space where the complex domain boundaries can be represented as a spherical boundary, without compromising the accuracy of the optimization. This solution is more advanced but also requires training the model with a sufficient number of samples.

In this article, we propose a new methodology to integrate multiple irregular, non-convex, and disconnected boundary constraints into the wind farm layout optimization problem. This method relies on polygon representation, given by the vertices of the polygons. The distance from every wind turbine to the polygons can be efficiently calculated by a set of geometric formulas that determine the nearest boundary and

the sign of the distance towards it. Based on the sign of this distance, it is always possible to identify if the wind turbine is inside or outside the considered polygon.

When this framework is used with gradient-based optimization, the wind turbines are placed within one of the inclusion zones around them within the first iterations, since the solver will try to satisfy all the constraints when the optimization is started. This means that the solution will be highly dependent on the initial positions. Additionally, if our inclusion zones consist of many polygons spread across the design space, conventional gradient-based optimization using multiple random starts may not be an effective approach to design wind farm layouts that fully utilize the available wind resource.

We have contemplated two possible solutions to overcome this challenge. The first solution is to introduce a term in the boundary constraint formulation that relaxes the problem by expanding or buffering the inclusion zone areas before the optimization is started. The use of larger inclusion zones means that more of the domain can be explored, and wind turbines can be placed around areas with better resources. During the optimization, the boundaries are “un-relaxed” linearly until they return to their true geometry. This is controlled with two parameters that model the offset per iteration and the number of optimization iterations in which the un-relaxation is applied. The second solution is the application of a heuristic algorithm, smart-start (Valotta Rodrigues et al., 2024), which takes a discretized grid covering the domain as input, removes all points outside the inclusion zones, and then iteratively adds turbines one by one. In each iteration the wake deficit from already-added turbines is calculated, and the next turbine is placed at the position with the highest power potential.

The presented framework has been implemented in TOP-FARM, the Technical University of Denmark’s (DTU’s) open-source software for wind farm optimization (Réthoré et al., 2014; DTU Wind Energy Systems, 2022b). A case study is presented, where the three introduced approaches are followed to maximize the annual energy production (AEP) of a wind farm in complex terrain with several irregularly shaped and disconnected inclusion zones. In this study, a gradient-based driver is combined with the relaxation of boundaries and with the smart-start algorithm to demonstrate the applicability of the method and how the aforementioned challenge can be overcome. For the AEP calculation and the wake modeling involved in the simulations, TOPFARM relies on PyWake (Pedersen et al., 2019), another DTU open-source Python library that offers fast AEP evaluation from a range of engineering wake models. Recent works using TOP-FARM (Ciavarra et al., 2022; Riva et al., 2020) and PyWake (Rodrigues et al., 2022; Fischereit et al., 2021; Forsting et al., 2021; Pedersen et al., 2021; Quick et al., 2023) can be found in the literature.

The article is structured as follows: Sect. 2 describes the mathematical principles and formulation of the method, in-

cluding the boundary relaxation; the idea behind smart-start; and how the flow is modeled along this work. Section 3 introduces the case study, describing in detail each of the approaches used and providing a relaxation study which was used to decide the suitable parameters for the second approach. Section 4 presents the results and discussion. Finally, Sect. 5 summarizes the conclusions and points towards future work.

2 Methods

Given a set of wind turbines, I , we wish to maximize the annual energy production (AEP) by finding the optimal layout of a farm. Our problem is constrained by a minimum distance between each pair of wind turbines and by several boundary constraints given as a set of disconnected polygons that are defined as inclusion or exclusion zones (i.e., the areas where the wind turbines are allowed or not allowed to be placed, respectively). Each polygon is formed by a number of boundary edges. This optimization problem is mathematically formulated as

$$\begin{aligned} & \max_{\mathbf{x}, \mathbf{y}} \text{AEP}(\mathbf{x}, \mathbf{y}) \\ & \text{s.t. } \sqrt{(x_i - x_j)^2 + (y_i - y_j)^2} \geq S_{\min}, \quad \forall i, j \in I : i \neq j \\ & \quad C_i \geq 0, \quad \forall i \in I \\ & \quad x_{\min} < x_i < x_{\max}, \quad \forall i \in I \\ & \quad y_{\min} < y_i < y_{\max}, \quad \forall i \in I, \end{aligned} \quad (1)$$

where \mathbf{x} and \mathbf{y} are the wind turbine coordinate vectors; x_{\min} , x_{\max} , y_{\min} , and y_{\max} are the lower and upper limits for the design variables; S_{\min} is the minimum distance between turbines; and the term C_i represents the signed distance from a wind turbine i towards the nearest boundary edge from the polygon set. In this context, signed distance means that if C_i is positive, the wind turbine is inside an inclusion zone or outside an exclusion zone, whereas if it is negative, the wind turbine is inside an exclusion zone or outside an inclusion zone. Although it might seem redundant to include design variable limits due to the fact that the boundary constraint is already acting as such, they are used in further sections to describe the methodology.

2.1 Distance to nearest polygon

In the aforementioned optimization problem (Eq. 1), a set of wind turbines and a set of polygons were given. The wind turbine locations are defined by their coordinates, and the polygons are defined by the coordinates of their vertices. The polygons can be split into boundary edges. Hence, any pair of adjacent vertices belonging to the same polygon forms a boundary edge. For example, two adjacent vertices of a polygon, with coordinates (x'_k, y'_k) and (x'_{k+1}, y'_{k+1}) , respectively, will form a boundary edge k , represented by a vector \mathbf{e}_k , whose components are defined as $(x'_{k+1} - x'_k, y'_{k+1} - y'_k)$. The

polygons follow a hierarchy that allows for the imposition of an exclusion zone on top of an inclusion zone and vice versa. If two or more of the same type of polygon overlap, these are merged into a single polygon, where the interceptions between boundary edges form the new vertices.

The main idea behind the method is to identify the nearest boundary edge from the wind turbine locations, calculate the distance to the nearest point on the respective boundary edge, and then compute the gradients of those distances with respect to the turbine locations to indicate the path that will lead them to the permitted areas. For this, a sequential approach is followed:

1. For each wind turbine, identify the nearest point on all boundary edges.
2. Compute the signed distances between each wind turbine and the identified nearest points, where positive distances mean inside an inclusion zone or outside an exclusion zone.
3. Identify the nearest edge (and polygon) by finding the minimum of the previously calculated signed distances, in absolute value.
4. Calculate gradients of the signed distance with respect to the wind turbine positions.

In addition, for each boundary edge, we define a normal unitary vector (a vector whose module is equal to the unit of length) that points inside the inclusion zone polygons and outside the exclusion zone polygons, as illustrated in Fig. 1. The purpose of the normal vectors is to indicate the correct side of the edge (where to place the turbines), and they are used to calculate the sign of the distances.

In order to mathematically formulate the method, we will demonstrate how to calculate the distance from a wind turbine i to an inclusion zone polygon of N vertices. The wind turbine location is defined by its coordinates (x_i, y_i) , and the polygon is defined by its vertex coordinates, $(x'_1, y'_1), (x'_2, y'_2), \dots, (x'_{N-1}, y'_{N-1}), (x'_N, y'_N)$. The polygon can be split into N boundary edges, $\mathbf{e}_1, \mathbf{e}_2, \dots, \mathbf{e}_N$. The last vector, \mathbf{e}_N , is defined from the last vertex (x'_N, y'_N) to the first one (x'_1, y'_1) , closing the polygon. In addition, for every boundary edge, we define the unitary normal vectors, $\mathbf{n}_1, \mathbf{n}_2, \dots, \mathbf{n}_N$, that point to the interior of the polygon, as it represents an inclusion zone (see Fig. 2).

The first step is to identify the nearest point from the wind turbine on all boundary edges. For this purpose, we define \mathbf{a}_{ik} as the vector from the first vertex of the boundary edge \mathbf{e}_k to the wind turbine location, and we define \mathbf{b}_{ik} as the vector from the second vertex of the boundary edge \mathbf{e}_k to the wind turbine location (notice that \mathbf{b}_{ik} is equivalent to $\mathbf{a}_{i,k+1}$). Now we can calculate \tilde{a}_{ik} , which is the projection of \mathbf{a}_{ik} into \mathbf{e}_k (Eq. 2), and \hat{a}_{ik} , which is the projection of \mathbf{a}_{ik} into \mathbf{n}_k (Eq. 3):

$$\tilde{a}_{ik} = \frac{\mathbf{a}_{ik} \cdot \mathbf{e}_k}{|\mathbf{e}_k|} \tag{2}$$

$$\hat{a}_{ik} = \mathbf{a}_{ik} \cdot \mathbf{n}_k. \tag{3}$$

Depending on the relative position of the wind turbine with respect to the boundary edge \mathbf{e}_k , we can distinguish three possibilities based on \tilde{a}_{ik} : (1) if \tilde{a}_{ik} is negative, the wind turbine is closer to the first vertex of the edge \mathbf{e}_k ; (2) if \tilde{a}_{ik} is positive and less than or equal to the length of the boundary edge, the wind turbine is closer to an intermediate point of the edge \mathbf{e}_k ; and (3) if \tilde{a}_{ik} is positive and larger than the length of the boundary edge, the wind turbine is closer to the second vertex of the edge \mathbf{e}_k . Figure 2 illustrates the different scenarios.

Once the nearest point on each boundary edge has been identified, the second step consists of computing the shortest signed distance between the wind turbine and the boundary edge. For case (2), this corresponds with the perpendicular distance, \hat{a}_{ik} . For cases (1) and (3), we need an additional vertex “normal” vector, $\mathbf{q}_1, \mathbf{q}_2, \dots, \mathbf{q}_N$, to calculate the correct sign of the distance. This vector is defined as the average of the normal unitary vectors of the adjacent boundary edges; i.e., the vertex “normal”, \mathbf{q}_k , of the vertex (x'_k, y'_k) is calculated as

$$\mathbf{q}_k = \frac{\mathbf{n}_k + \mathbf{n}_{k-1}}{2}. \tag{4}$$

The vector \mathbf{q}_k points to the “correct” side of the vertex. This means that the sign of the projection \mathbf{a}_{ik} on \mathbf{q}_k , $\sigma_{ik} = \text{sign}(\mathbf{a}_{ik} \cdot \mathbf{q}_k)$, is positive if the turbine is inside an inclusion zone and outside an exclusion zone and vice versa if the projection is negative. To summarize, the signed distances D_{ik} from all wind turbines i to all boundary edges k of all inclusion- and exclusion-zone polygons are calculated as

$$D_{ik} = \begin{cases} |\mathbf{a}_{ik}| \sigma_{ik}, & \text{if } \tilde{a}_{ik} < 0 \\ \hat{a}_{ik}, & \text{if } \tilde{a}_{ik} \geq 0 \text{ and } \tilde{a}_{ik} \leq |\mathbf{e}_k| \\ |\mathbf{b}_{ik}| \sigma_{ik}, & \text{if } \tilde{a}_{ik} > |\mathbf{e}_k| \end{cases}. \tag{5}$$

Note, in the second case in Eq. (5), the sign is implicit in \hat{a}_{ik} .

Hereafter, we can proceed with the next step, which consists of identifying the nearest boundary edge (of the nearest polygon). This is done by

$$\mathbf{C}_i = \min_k (|D_{ik}|) \cdot \text{sign}(D_{ik}), \tag{6}$$

which calculates a vector \mathbf{C} , whose components represent the distance between each turbine and their respective nearest boundary edge. This vector is the term in the inequality constraint in Eq. (1). The gradient of \mathbf{C} will define the right direction to go for every wind turbine to be placed within an inclusion zone and outside exclusion zones to meet the

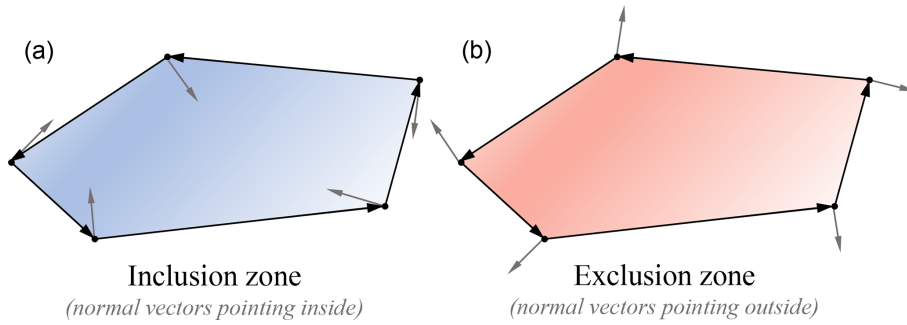


Figure 1. Definition of the polygon depending on the inclusion or exclusion attribute. (a) Normal unitary vectors pointing inside the polygon, representing an inclusion zone, (b) normal unitary vectors pointing outside the polygon, representing an exclusion zone.

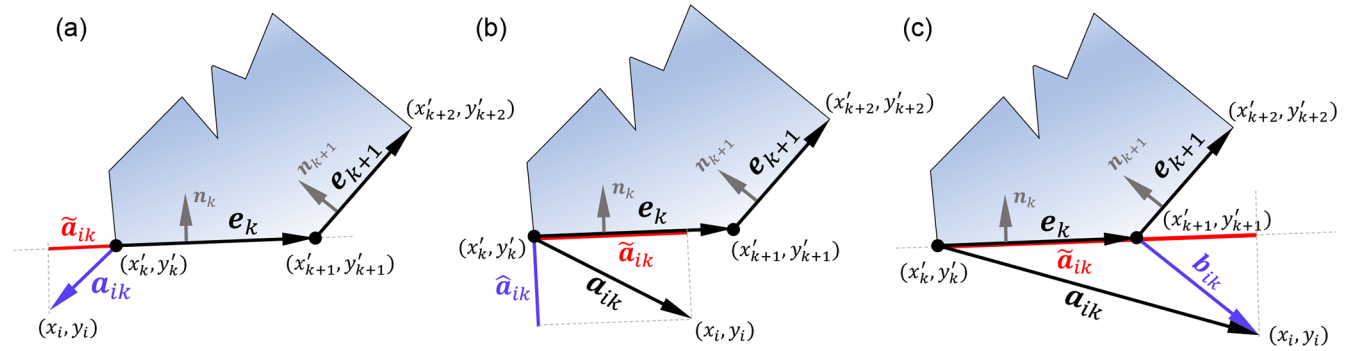


Figure 2. (a) Wind turbine i is closer to the first vertex of the boundary edge e_k (case 1). (b) Wind turbine i is closer to an intermediate point of the boundary edge e_k (case 2). (c) Wind turbine i is closer to the second vertex of the boundary edge e_k (case 3). The red lines, \tilde{a}_{ik} , correspond to the projection of a_{ik} on boundary e_k , while the blue lines/vectors correspond to the shortest distance between turbine i and the boundary edge e_k .

boundary constraint. The analytical gradients of C with respect to the wind turbine coordinates can be written as follows:

$$\frac{\partial C_i}{\partial x_i} = \begin{cases} \frac{x_i - x'_k}{\sqrt{(x'_k - x_i)^2 + (y'_k - y_i)^2}} & \text{if } \tilde{a}_{ik} < 0 \\ \frac{y'_k - y'_{k+1}}{\sqrt{(x'_{k+1} - x'_k)^2 + (y'_{k+1} - y'_k)^2}} & \text{if } \tilde{a}_{ik} \geq 0 \text{ and } \tilde{a}_{ik} \leq |e_k| \\ \frac{x_i - x'_{k+1}}{\sqrt{(x'_{k+1} - x_i)^2 + (y'_{k+1} - y_i)^2}} & \text{if } \tilde{a}_{ik} > |e_k| \end{cases} \quad (7)$$

$$\frac{\partial C_i}{\partial y_i} = \begin{cases} \frac{y_i - y'_k}{\sqrt{(y'_k - y_i)^2 + (x'_k - x_i)^2}} & \text{if } \tilde{a}_{ik} < 0 \\ \frac{x'_{k+1} - x'_k}{\sqrt{(x'_{k+1} - x'_k)^2 + (y'_{k+1} - y'_k)^2}} & \text{if } \tilde{a}_{ik} \geq 0 \text{ and } \tilde{a}_{ik} \leq |e_k| \\ \frac{y_i - y'_{k+1}}{\sqrt{(x'_{k+1} - x_i)^2 + (y'_{k+1} - y_i)^2}} & \text{if } \tilde{a}_{ik} > |e_k| \end{cases} \quad (8)$$

Note that $\frac{\partial C_i}{\partial x_j} = 0$ when $i \neq j$ and that, in Eqs. (7) and (8), k is set as $\underset{k}{\operatorname{argmin}}(|D_{ik}|)$.

In general, the distances between the wind turbines and the boundaries are continuous and differentiable but not continuously differentiable. When the nearest edge with respect to a wind turbine switches from one edge to another, the gradi-

ent will make a discontinuous jump, but this does not seem to be an issue for the used solver (see details of the solver in Sect. 3).

The gradient-based solver sequential least-squares programming described by Kraft (1988), from now on SLSQP, was used for the numerical experiments, as implemented in the Python library, SciPy (Virtanen et al., 2020). The running time of the algorithm scales linearly with both the number of wind turbines and the number of boundary edges ($N_{WT} \cdot N_{edges}$).

2.2 Distance relaxation

The described methodology to include multiple polygons in our optimization domain means that solvers, which seek to obtain a feasible solution immediately after the optimization is started, will try to satisfy the inequality constraint, $C_i \geq 0$, by placing all the wind turbines inside the nearest polygon. Moreover, once a wind turbine is inside a polygon, it will not be able to explore the rest of the design space as it would violate the boundary constraint, and therefore the number of wind turbines allocated in each polygon will depend on the initial positions.

A potential solution for this is to relax the problem by expanding the boundary constraints for a certain number of iterations. This allows for a deeper exploration of the design space at the beginning of the optimization and thus a more suitable distribution of the wind turbines between the existing polygons. When the relaxation is applied, an initial maximum offset is added up to the inclusion zone boundaries. Once the optimization is started, this maximum offset is gradually removed (the problem is “un-relaxed”) at a constant rate. The un-relaxation is ruled by a linear expression that describes the relation between the relaxed distances, R_{ik} , and the iteration number, γ :

$$R_{ik} = \begin{cases} D_{ik} + k_r(\gamma_r - \gamma), & \text{if } \gamma < \gamma_r \\ D_{ik}, & \text{if } \gamma \geq \gamma_r \end{cases}, \quad (9)$$

where the first parameter, k_r , defines the added offset per iteration and the second parameter, γ_r , defines the number of iterations during which the un-relaxation lasts. With this implementation, the largest offset, $k_r \cdot \gamma_r$, occurs at the beginning of the optimization and is gradually reduced until the maximum number of iterations for relaxation, γ_r , is reached.

For a better understanding of the distance relaxation, its application has been illustrated in Fig. 3. In the example, a simple set of polygons representing five inclusion zones is relaxed, applying an offset of 5 m per iteration ($k_r = 5$) during 160 iterations ($\gamma_r = 160$). The iteration number is given by γ , illustrated in the title of each plot. In the first iteration ($\gamma = 1$), the boundaries are relaxed with the maximum offset, which is beyond the limits of our domain; thus the relaxed polygons cannot be seen in the plot. The design variables are only limited by their respective upper and lower bounds, meaning that the solver can freely move them within the whole domain, illustrated by the dashed red line. When $\gamma = 100$, the relaxed polygons start to gradually push the wind turbines towards the inclusion zones as the optimization progresses. The plots for $\gamma = 130, 140$, and 150 illustrate this process in which the relaxed boundaries are shrunk (un-relaxed) until they reach their default shapes. Eventually, for $\gamma = 160$, the un-relaxation ends, and all wind turbines will be allocated inside a polygon.

When distance relaxation is applied, the nearest boundary is determined as

$$C_i = \min_k (|R_{ik}|) \cdot \text{sign}(R_{ik}), \quad (10)$$

which is a vector of the nearest distances between each turbine and the relaxed boundaries.

The distance relaxation allows for a better exploration of the design space. It can also be applied to escape from the local optimum or to allow transferring of wind turbines between polygons for a certain number of iterations.

2.3 Smart-start algorithm

Another method to solve the wind turbine allocation problem is to discretize the domain and place the wind turbines in the inclusion zone polygons before the optimization is launched. The smart-start algorithm, implemented in PyWake as in Valotta Rodrigues et al. (2024), is meant to get a better initial layout of a wind farm. A diagram depicting the rationale of the algorithm is presented in Fig. 4. The idea is to sequentially place the wind turbines one by one in the positions with the best wind resource, taking wake effects of the previously added wind turbines and boundary and spacing constraints into account.

The algorithm takes a list of discretized potential wind turbine locations, \mathcal{L} , as input, and, after removing all locations where the boundary constraints are violated, the main loop starts. In each iteration the wind resource, including wake effects from already-added wind turbines, is evaluated at all points in \mathcal{L} , and the next wind turbine is added at the location that yields the highest AEP. This means that the reduction in AEP of the previously added turbines is not considered. Hence, the solution may not be optimal, but it implies a crucial reduction in computational costs. After adding the next wind turbine, all points where the spacing constraints are not satisfied are removed from \mathcal{L} , and the algorithm continues until all wind turbines are added.

The algorithm has been extended with a randomness parameter r that allows it to put the next turbine at one of the n best positions by random, where $n = \max(r \cdot \text{size}(\mathcal{L}), 1)$.

The r parameter ranges between 0, which corresponds to always picking the best position, and 1, which corresponds to a completely random choice of points.

The performance of smart-start depends on the number of potential locations (grid resolution): a very high resolution grid will involve high computational effort, while a coarse resolution might lead to inefficient wind turbine allocation.

2.4 Flow modeling

When a site has complex terrain, like mountains and valleys, the landscape creates changes in pressure that result in changes in the local wind speed. This section explains how the wind resource and the flow are modeled along the case study. The wind farm is modeled using a flow map describing the local wind conditions. The local directions and speeds are dependent on the spatial location; the freestream wind speed, U_∞ ; the freestream wind direction, θ_∞ ; and local velocity deficits from wake losses. The local wind speed and direction can be expressed as

$$U_{iud} = U_{\infty u} \cdot s_{id} \quad (11)$$

$$\theta_{id} = \theta_{\infty d} + t_{id}, \quad (12)$$

where the terms s_{id} and t_{id} represent the wind speedups and turning, respectively, at a location i and for a freestream direction d ; U_{iud} represents the local wind speed for a

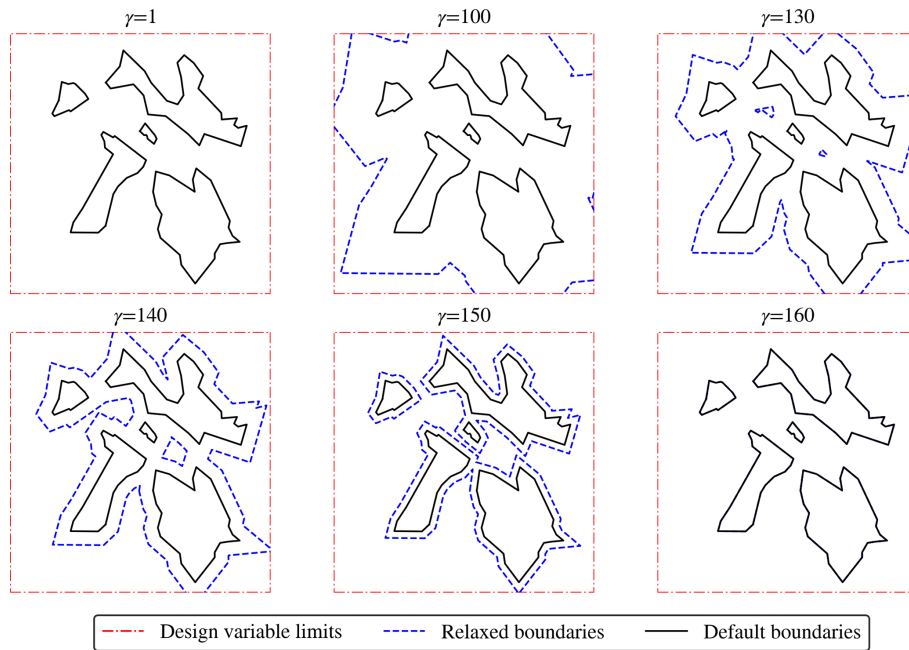


Figure 3. The optimization boundary constraint is visualized for different optimization iterations when using the distance relaxation method in a hypothetical problem with $k_r = 5$ and $\gamma_r = 160$. The solid black lines denote inclusion zone boundaries; the dashed red lines show the domain limits, defined by the upper and lower bounds of the design variables; and the dashed blue lines represent the relaxed boundaries, which change depending on the iteration number γ . Each plot shows a different optimization iteration number.

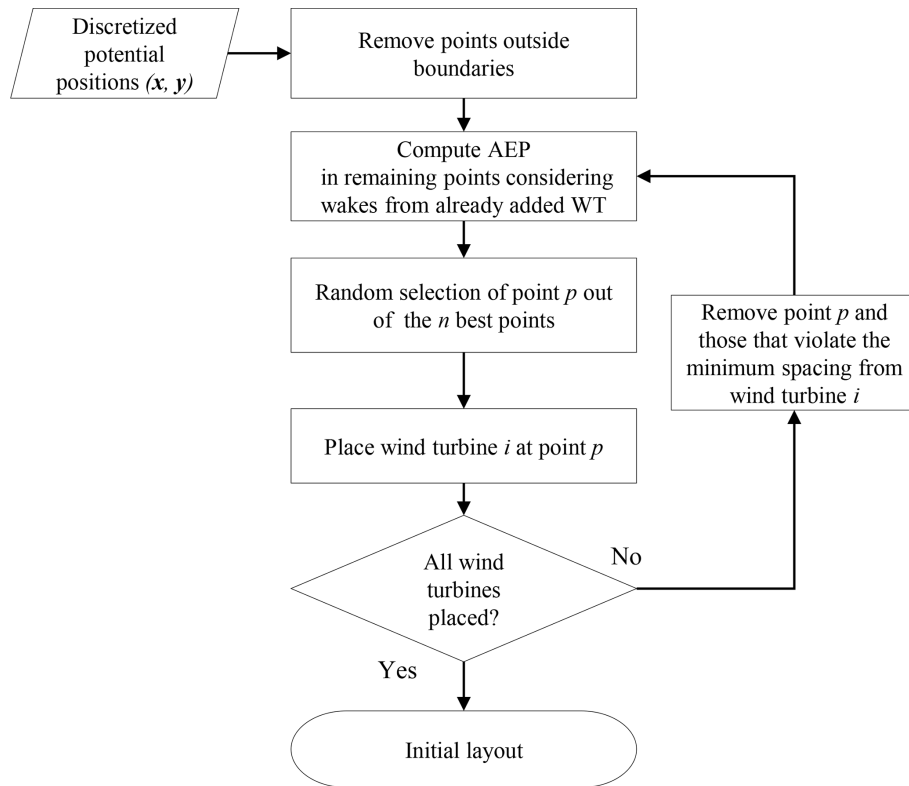


Figure 4. Workflow visualization of the smart-start algorithm.

freestream wind speed u , affected by the orography speedup effects; and θ_{id} represents the local wind direction, affected by the orography turning effects. Notice that the speedup and turning are independent from the freestream wind speed. The local wind speed has to include the deficits derived from wind turbine interactions, Δu_{iud} , which are imposed as

$$u_{iud} = U_{iud} - \Delta u_{iud}. \tag{13}$$

In this study, the objective function of the optimization is the annual energy production or AEP. For each set of inflow conditions, the individual turbine powers are summed according to the probability of $(U_{\infty u}, \theta_{\infty d})$,

$$AEP(x, y) = 8760 \sum_{d=1}^{N_\theta} \sum_{u=1}^{N_u} \sum_{i=1}^{N_{wt}} P(u_{iud}) \rho(U_{\infty u}, \theta_{\infty d}), \tag{14}$$

where ρ is the probability mass function; N_{wt} is the number of wind turbines; P is the power curve function; and u_{iud} is the local velocity, including wake effects, associated with freestream direction $\theta_{\infty d}$, wind speed $U_{\infty u}$, and turbine position (x_i, y_i) .

The wake effects are approximated using the Bastankhah Gaussian wake deficit model (Bastankhah and Porté-Agel, 2014). This model is derived from the mass and momentum conservation and assumes a Gaussian distribution of the velocity deficits in the wake, controlled by a single parameter k^* to model the expansion. The velocity deficit from wind turbine j on wind turbine i is estimated by the expression below:

$$\Delta u_{ijud} = U_{iud} \left(1 - \sqrt{1 - \frac{C_T}{8(k^* \Delta_{ijd}^x / d_0 + \varepsilon)^2}} \right) \exp \left\{ \frac{-1}{2[k^* \Delta_{ijd}^x / d_0 + \varepsilon]^2} \left[\left(\frac{\Delta z_{ij}^H}{d_0} \right)^2 + \left(\frac{\Delta_{ijd}^y}{d_0} \right)^2 \right] \right\}, \tag{15}$$

where k^* is the expansion parameter (for this study, a value of 0.032 was used); d_0 is the rotor diameter of the wind turbines; Δ_{ijd}^x and Δ_{ijd}^y are the upstream and crosswind distances between turbines i and j , respectively; Δz_{ij}^H is the hub height difference between turbines i and j ; C_T is the thrust coefficient; and ε is the standard deviation of the Gaussian profile, normalized with the rotor diameter, very close to the upstream wind turbine, i.e., where $\Delta_{ijd}^x \approx 0$.

In this study, Δ_{ijd}^x is computed as the length of the line that follows the terrain (i.e., has a constant height above the ground) from the upstream to the downstream wind turbine projected onto the downwind direction axis, Δ_{ijd}^y is the straight crosswind distance (currently the method does not consider the terrain variations in the crosswind direction), and Δz_{ij}^H is zero, as all the wind turbines have the same hub height.

The resulting velocity deficit fields are calculated by adding up the deficits from the upstream wind turbines using a squared sum wake superposition model,

$$\Delta u_{iud} = \sqrt{\sum_{\forall j: \Delta_{ijd}^x > 0} \Delta u_{ijud}^2}, \tag{16}$$

where the notation $\Delta_{ijd}^x > 0$ ensures that the velocity deficits are only accounted for downstream distances.

The wind turbine model used for this work is based on the Vestas V80-2.0, which has a rotor diameter of 80 m, a hub height of 70 m, and a nominal power of 2 MW. The power and thrust curves for this model are pre-defined in PyWake.

3 Application

In this section, we present a case study based on a fictitious site, Parque Ficticio, with complex terrain. The site is featured by a non-uniform wind resource and a terrain elevation map. The purpose of the study is to show a wind farm layout optimization using gradient-based methods and demonstrating the performance of the multi-polygon boundary constraint described in the prior section of this work. The results from three different optimization approaches are compared and assessed.

3.1 Optimization setup

A wind farm consisting of 12 wind turbines is optimized following the formulation described in Eq. (1), where the design variables are the wind turbine locations and the constraints comprise a minimum spacing of two rotor diameters (equivalent to 160 m) between wind turbines and five irregular inclusion zone polygons (see Fig. 5). The AEP is calculated as described in Sect. 2.4, considering local wind directions, local wind speeds, and wake effects, as defined by Eqs. (11)–(13).

3.2 Site description

Parque Ficticio is a fictitious wind farm site pre-defined in PyWake, where the wind resource and terrain data are given as a dataset whose coordinates are x (UTM easting projection), y (UTM northing projection), h (height), and wd (wind direction sector). The wind resource is characterized by a unique Weibull distribution per wind sector (12 sectors). The dataset contains a gridded map of speedups and turning values that change with the sector. Note that, although the site has a resolution of 12 wind sectors, the bin resolution for the optimization is thinner, which means that wake losses will be optimized with 1° precision despite the fact that the frequency of certain inflow conditions is assumed to be the same.

At the site, we have defined five potential inclusion zone polygons, as seen in Fig. 5, where the wind turbines are allowed to be installed. From the wind rose in Fig. 5, it can be

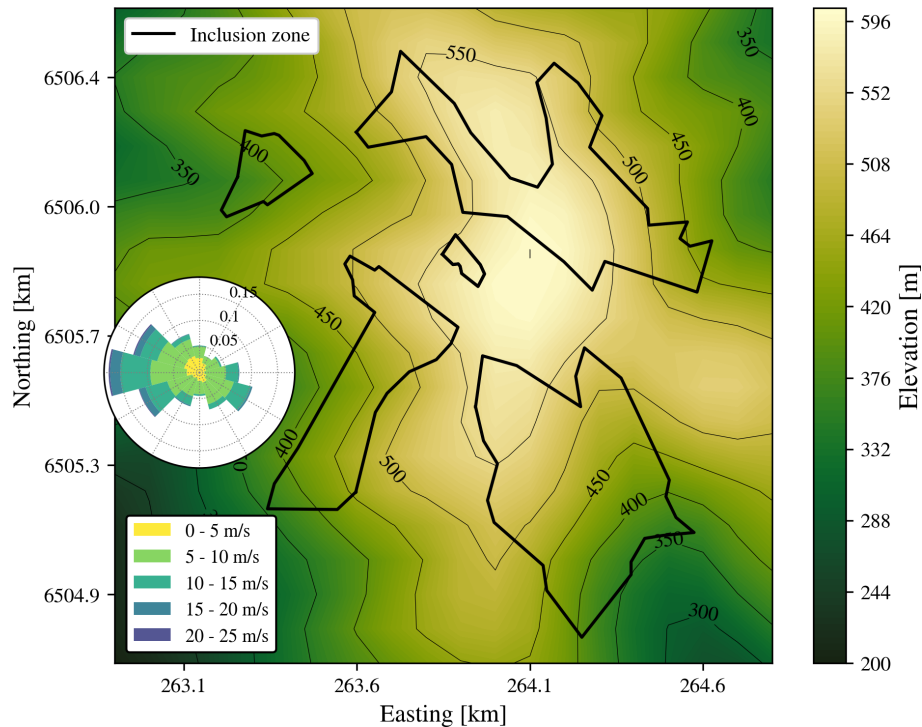


Figure 5. Parque Ficticio site is considered in this study. The elevation is shown with colors in contours. The inclusion zones are shown in thick dark lines. The illustrated wind rose shows the sector and wind speed frequency according to the freestream probabilities, which change locally due to orographic effects.

observed that the site has dominant westerly winds. The local winds are affected by the terrain effects, such as speedups and turning.

3.3 Approaches to optimization of the layout

The wind farm is optimized following three independent approaches. The initial positions of the wind turbines are randomized using predetermined random number generator seeds to ensure that the results are reproducible. Altogether, 50 seeds (from 1 to 50) were run for each of the three approaches. For all approaches, the gradient-based solver SLSQP was used. The discretized wind directions and wind speeds for the optimizations were 1° and 1 m s^{-1} bins, respectively. We set a limit of 500 iterations with a tolerance for convergence of 10^{-6} on the objective function.

The optimizations were run in an HPC cluster (Technical University of Denmark, 2019) to allow parallelization. Every case was performed in an individual node composed of 2×16 AMD EPYC 7351 2.9 GHz processors and 128 GB RAM. The numerical computations were parallelized using the full node capacity. A new Anaconda environment (ana, 2020) was created with the required Python libraries (see “Code and data availability” for further information about Git repositories and used commits). When performing AEP computations, PyWake allows “chunkification”, which distributes the flow cases between the available resources in

batches of wind directions and wind speeds, resulting in a reduction of the computational times. In our simulations, the wind direction flow cases were divided into 32 wind direction chunks.

The different approaches for optimization using gradient-based solvers and the implemented techniques are described below:

- *Approach 1* (SLSQP). The gradient-based solver SLSQP is used for the optimization. The Jacobians were calculated using automatic differentiation with the Python library *autograd* (Maclaurin et al., 2015). This same setup is used for the remaining approaches combined with other optimization techniques.
- *Approach 2* (relaxation + SLSQP). The distance relaxation as described in Sect. 2.2 is applied during the first γ_r iterations of the optimization. This allows the solver to freely move the wind turbines around the whole design space, leading to their better allocation between the different inclusion zones. The values of k_r and γ_r have to be selected according to the size of the domain and of the inclusion zone areas. Although there is not a rule of thumb or any related heuristics for this purpose, general guidance is that the more spread the inclusion zones are, the larger the values of the parameters should be. A relaxation study was done to select suitable values for

the case study (see Sect. 3.4) resulting in $k_r = 100$ and $\gamma_r = 100$.

- *Approach 3* (smart-start + SLSQP). The smart-start algorithm is applied to achieve a better initial layout. This involves all the initial positions being inside the inclusion zones at the beginning of the optimization. A 10% randomization is used, which means that the positions are subsequently selected randomly out of the best 10% of available points. For this randomization, the indicated seeds are applied. The domain is discretized with a grid of 100×100 points. After smart-start is executed, SLSQP is used as in the other two approaches. No distance relaxation was applied for this case.

The idea behind using these different approaches is to (1) demonstrate that the nearest distance method succeeds in placing the wind turbines inside the inclusion zones in a wind farm layout optimization problem; (2) demonstrate how the distance relaxation is able to achieve higher-quality solutions by avoiding local optimum caused by the discontinuity of the boundaries; and (3) show the advantages of using the smart-start algorithm to initialize the wind farm layout optimization problem with multiple boundaries, as it efficiently allocates the wind turbines between the inclusion zones.

3.4 Relaxation study

As described in Sect. 2.2, k_r defines the offset per iteration, and γ_r indicates the maximum number of iterations for relaxation. k_r can also be seen as the “speed” of un-relaxation, while γ_r can be seen as the “duration” of the relaxation. If these parameters are too small, the relaxation will not be effective, as the extension of the allowed area is too small, or there might not be enough iterations to explore the domain. On the other hand, if one of these parameters is too large, the optimization may converge before the boundaries are back to their true shapes, involving the risk of reaching a constraint-violating solution.

A parametric study was done in order to find a suitable combination of values that would lead to the higher potential yield for the case study. Four combinations of values for k_r and γ_r were chosen: combinations 1, 2, and 3 compare the impact of different un-relaxation speeds for a fixed number of iterations before the last 300 m is un-relaxed (from 300 m on, the changing boundaries begin to push the wind turbines towards the true boundaries). These combinations satisfy the expression

$$\gamma_r = \frac{300}{k_r} + 100, \quad (17)$$

which ensures 100 iterations of optimization before the un-relaxation is applied to the last 300 m. In other words, the solver has 100 iterations to distribute the wind turbines within a sufficiently large area to find positions where the

Table 1. Failed seeds for the relaxation study.

Relaxation strategy	Number of failed seeds	Percentage (%)
$k_r = 2, \gamma_r = 250$	12	24
$k_r = 5, \gamma_r = 160$	6	12
$k_r = 100, \gamma_r = 100$	3	6
$k_r = 2, \gamma_r = 100$	1	2

wind resource is higher before the last part of the un-relaxation happens. The selected k_r values were 2, 5, and 100 (in the case of $k_r = 100$, γ_r would be 103 to satisfy Eq. (17), but it was rounded down to 100).

Combinations 3 and 4 compare the impact of different un-relaxation speeds for fixed relaxation iterations with the idea of exploring the impact of the relaxation maximum offset (i.e., a low value against a high value of k_r keeping a constant γ_r). The selected values for combination 4 were $k_r = 2$ and $\gamma_r = 100$, compared to combination 3 with $k_r = 100$ and $\gamma_r = 100$.

A total of 50 optimizations were run for each of the selected combinations. Some of the seeds were filtered as they resulted in constraint-violating solutions, as a local minimum is found before the un-relaxation finishes and the solver stops. More specifically, Table 1 shows the percentage of seeds that failed to reach constraint-satisfying solutions. In total, 17 out of the 50 seeds failed in at least one of the combinations and were filtered out; thus the final sample for this relaxation study contains 33 seeds that run successfully for all combinations of relaxation parameters. Figure 6 shows the AEP of the 33 runs during the optimization as a function of iteration number. The dashed lines in each plot indicate the iteration where the boundaries return to their actual shapes, and a different color is used for each seed. When the optimizations are launched, it can be seen how the AEP increases quickly due to the effect of relaxation. When the wind turbines start to find positions that are close to the local optimum, a plateau is formed for the curves (the plateau shape can be observed more clearly for the first plot, for $k_r = 2$ and $\gamma_r = 250$). Afterwards, when the relaxed boundaries get closer to the default inclusion zone polygons, the slope of the AEP curve becomes negative, as the turbines are forced to leave those already-found sweet spots and are pushed inside the smaller allowed areas. Depending on the value of k_r , this slope is more or less steep: notice that for the lower-left plot ($k_r = 100$ and $\gamma_r = 100$), this slope is almost vertical, as the last 300 m of un-relaxation occurs in only 3 iterations (which would be very similar to removing the boundary constraints for the first 100 iterations of the optimization and activating them afterwards).

Figure 7 shows the statistics from this study using violin plots, where the mean and the first and third quantiles are represented. There are two remarkable facts that can be inferred from this plot: firstly, for combinations 1–3 (k_r/γ_r cor-

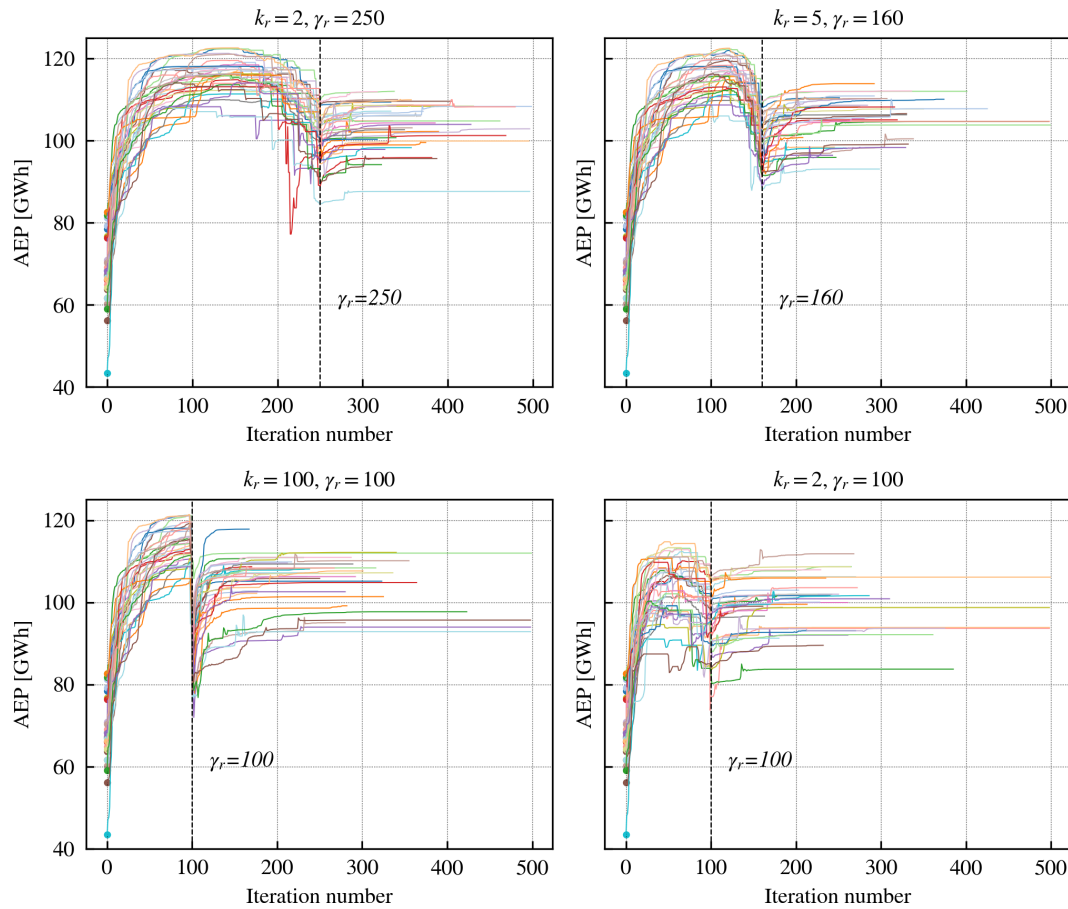


Figure 6. AEP convergence as a function of the iteration number for each of the studied relaxation combinations. The multicolored lines correspond to the different seed numbers.

responding to 2/250, 5/160 and 100/100) the mean of combination 3 with the fastest un-relaxation is slightly higher, but all distributions are relatively similar. Based on this, we can state that there is no clear benefit in slowing down the un-relaxation; i.e., instantly activating the constraints after 100 iterations performs at least as well as a more gradual relaxation strategy. Secondly, from the last two combinations (k_r/γ_r corresponding to 100/100 and 2/100) we can conclude that the number of iterations before relaxing the last 300 m has an impact on the result, as for too small a k_r , the maximum offset is not sufficiently large enough for the solver to find good positions for the turbines before the boundaries are back to their default shapes.

Based on this relaxation parametric study, it was decided that $k_r = 100$ and $\gamma_r = 100$ would be used as parameters for the relaxation approach, as this combination gives slightly higher AEP and fewer constraint-violating results.

4 Results

In this section, the results from the optimizations that were run following the described approaches are presented. De-

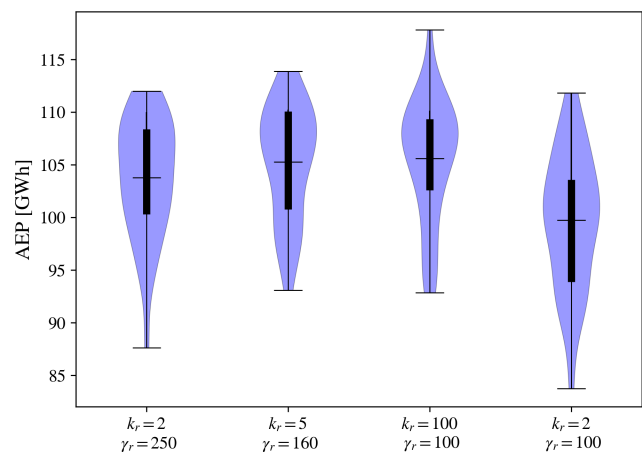


Figure 7. Relaxation study statistical summary. The violin plots illustrate the distribution of results from the 33 seeds. The black bars indicate the first and the third quartiles of the sample. The horizontal lines represent the means.

Table 2. Failed seeds for the different approaches.

Optimization approach	Number of failed seeds	Percentage (%)
SLSQP	5	10
Relaxation + SLSQP	3	6
Smart-start + SLSQP	0	0

spite the fact that most of the optimizations converged successfully, there were a few cases where they reached the maximum number of iterations before convergence; these were considered valid if all the wind turbines satisfied the boundary and the distance constraints. On the other hand, some seeds led to an infeasible solution for some of the approaches; in these cases, the seed was not considered for the final results. In total, eight seeds had to be removed from the results for this reason, as shown in Table 2. More specifically, the next events were the reason for discarding them:

1. SLSQP showed constraint violations after reaching the maximum number of iterations in seeds 9, 21, 22, and 33. This means that the solver is not able to place all the wind turbines within the inclusion zones while complying with the spacing constraint at the same time.
2. In seeds 3 and 26, SLSQP + relaxation converges before the boundaries are back to their true shape; i.e., the optimization finishes in fewer iterations than the maximum number of iterations for relaxation, leading to an unfeasible solution.
3. Approach 1 fails due to the incompatibility of inequality constraints before reaching the limit of iterations in seed 29. This means that the solver is not able to place all the wind turbines within the inclusion zones while complying with the spacing constraint at the same time. Also, it is not able to find new positions for the turbines that are violating the constraints.
4. Approach 2 fails in seed 41, as SLSQP fails to find a constraint-satisfying solution.

From the 42 remaining seeds, the first approach achieved an average AEP value of 95.55 GWh, with a standard deviation of 8.04 GWh. Approach 1 took an average of 207 iterations to finish and an average time of 152 s. The convergence of the different seeds is illustrated in Fig. 8.

With the second approach, an AEP average value of 105.3 GWh was yielded, with a standard deviation of 5.49 GWh. This involves an increase of +10.2 % of the AEP compared to the first approach. Approach 2 took an average of 303 iterations to finish and an average time of 180 s. The convergence of the different seeds is illustrated in the center plot of Fig. 8. Until iteration 100, the AEP increases significantly, as the boundaries are relaxed and the solver can find wind turbine positions in areas with higher resource; however, when the boundaries go back to their default shapes,

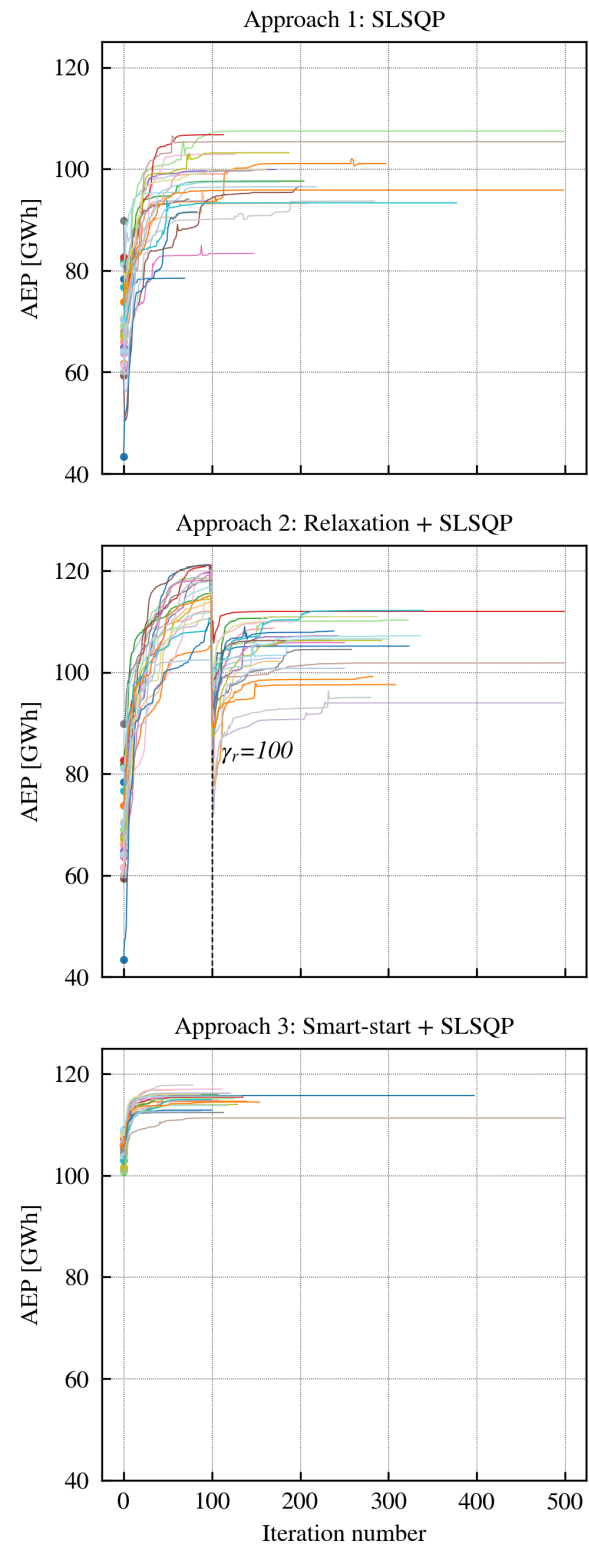


Figure 8. AEP plotted as a function of the iteration number of each optimization approach examined. The multicolored lines correspond to the different seed numbers.

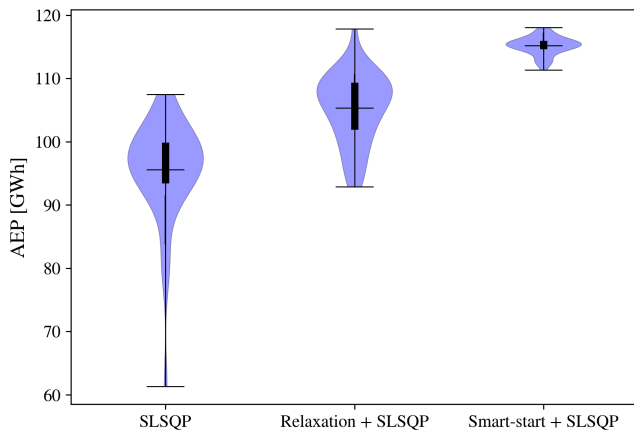


Figure 9. Violin plots depicting the distribution of AEP found through the different optimization approaches using 42 random starting locations.

some of the areas with good resource become restricted, and the solver has to seek new ones inside the inclusion zones. The abrupt decay in the AEP happens in a few iterations due to the high speed of the relaxation, as was shown in the relaxation study (Sect. 3.4).

The third approach achieved an average AEP value of 115.17 GWh, with a standard deviation of 1.43 GWh. This involves an increase of +20.53 % with respect to the first approach and +9.37 % with respect to the second approach. This approach took an average of 149 iterations to finish and an average of 118 s, which includes the time required to compute smart-start (on average 3 s using a regular grid of 100×100 , which corresponds to spacing each point 2.375×10^{-1} rotor diameters in each direction, x and y). The faster convergence with respect to the other approaches is due to starting the optimization from feasible positions that already provide a good AEP, from which the gradients can find the local optimum easier.

Figure 9 shows a graphical summary of the statistics described above. The approaches subsequently achieve a higher AEP on average. The tail of the distribution for approach 1 is longer due to finding a local sub-optimum, but most of the seeds tend to find an optimum around the mean. The standard deviation decreases remarkably when using the smart-start algorithm, as many sub-optimal solutions are avoided. These results demonstrate that the technical limitations of the method can be overcome with the relaxation of boundaries, and, moreover, the initialization of the layout with smart-start provides better solutions than using random guesses all over the domain. On top of that, smart-start converges faster towards the solution, requiring on average 27 % to 35 % less time when compared to the other approaches.

Figure 10 illustrates an example of the final layouts achieved by one of the seeds (number 11), which is representative of an average result. The contours in the background represent the mean wind speed at the hub height. The loca-

tions with higher resource in the map correspond to the areas with higher elevation, and, looking back to Fig. 5, it can be recalled that the wind has majorly a westerly component, which explains why the wind turbines tend to align in the vertical direction. The legend in each of the plots indicates the total AEP achieved by the layout, and the dotted red circles represent the minimum spacing constraint.

At first glance, it can be noticed that the allocation of wind turbines is better when the relaxation or smart-start is applied. In the layout achieved by approach 1 (left-hand plot in Fig. 10), the discontinuities between different inclusion zones increase the odds for the solver to become stuck in local minimum, which results in the baseline approach often failing to allocate the wind turbines in areas with higher resource. An instance of this is the four wind turbines in the lower-left inclusion zone: despite the wind resource being lower than in other areas, the solver opts to place the wind turbines in that polygon as it was nearest to their initial positions, and, during the optimization, these wind turbines do not leave the polygon, as it would violate the boundary constraint unless they manage to jump into another inclusion zone.

The relaxation of boundaries skips this local optimal trap temporarily and, as a result, achieves an improvement in the farm AEP (middle plot in Fig. 10). It can be observed that in the same inclusion zone (lower-left polygon) there are three fewer wind turbines than for approach 1. The result of this is a significantly higher yield, leading to an AEP of 107.15 GWh (+7.25 % with respect to approach 1).

The smart-start algorithm beats boundary discontinuity in a different way: the wind turbines are placed one by one in the positions with best resource, leading to an initial feasible solution which, despite not allowing wind-turbine transferring between the inclusion zones, already provides a good distribution of wind turbines within the available polygons. In this particular case, it can be seen how approach 3 (right plot in Fig. 10) allocates more wind turbines where the yield potential is higher.

In general, the use of smart-start to find a better initial layout before the optimization proved to achieve higher-quality solutions; the relaxation applied during a number of iterations when the optimization is started helps in getting higher values of AEP when compared to the use of SLSQP alone.

5 Conclusions and future work

This article describes a new method to include multiple boundary constraints represented by polygons in wind farm layout optimization problems. The method relies on the nearest distance from the wind turbine positions to the polygons. The sign of the distance determines if the wind turbine is inside or outside of the polygon. A positive sign involves the wind turbine being inside an inclusion zone or outside an exclusion zone and vice versa for a negative sign. A new in-

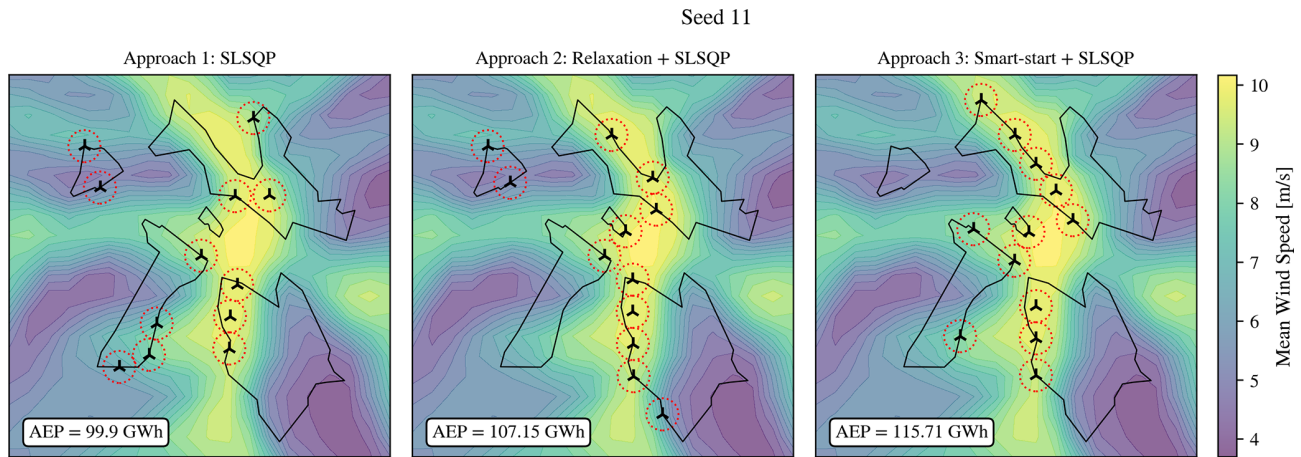


Figure 10. Final layouts, seed 11. The contour colors in the background indicate the mean wind speed over the site. The legend indicates the AEP for each of the resulting layouts for this seed. Approaches 2 and 3 succeed in placing more wind turbines over the yellow areas, where the mean wind speed is higher, leading to better solutions.

equality constraint is introduced in the optimization formulation to force the wind turbines to stay within the desired polygons.

Despite a limitation of this methodology being identified, which relates to the correct allocation of wind turbines between polygons, two potential solutions are proposed: the implemented boundary constraints can be relaxed during a definite number of iterations to allow a better exploration of the domain and consequently find a better allocation of turbines; alternatively, a heuristic algorithm can provide a better initial guess that saves computational time and achieves higher-quality solutions.

To demonstrate the applicability of the method and the effectiveness of the proposed solutions to its limitation, a case study was presented. A wind farm consisting of 12 wind turbines at a site with non-uniform wind resource and elevation was optimized using three different approaches: approach 1 consisted of using a gradient-based solver, while approaches 2 and 3 were subsequent combinations of the same solver with the boundary relaxation and the smart-start algorithms, respectively. For the numerical computations, the open-source Python libraries developed by DTU Wind and Energy Systems, TOPFARM and PyWake, were used.

The results show that the distance method successfully respects the boundaries of the given irregularly shaped and disconnected polygons, although, for certain initial conditions, incompatibility between the spacing and the boundary constraints might lead to an unfeasible solution. A parametric study for the relaxation was carried out with four combinations of parameters to decide the most suitable values that would be used in the case study. This demonstrated that the speed of relaxation does not have a significant impact on the results, but there has to be enough time for the solver to place the wind turbines around the areas with higher resource. In general, the relaxation of boundaries proved helpful in find-

ing a better optimum layout and wind turbine distribution between the inclusion zones. An average improvement of +10.2% in the AEP gain was achieved by approach 2 with respect to the sole use of gradients to solve the optimization problem. Moreover, the combination of heuristic optimization methods such as the smart-start algorithm, with gradient-based solvers followed by approach 3, reached even higher-quality solutions while saving some computational time. The average improvement of approach 3 with respect to the other approaches was +20.53% and 9.37%, respectively.

In future work, the method should be tested under more realistic scenarios, with a higher number of inclusion zone polygons and wind turbines, which increase the computational cost substantially. We observe that the time taken by SLSQP to handle constraints becomes significantly longer around 10 000 constraints. Furthermore, the comparison of the described approaches could be investigated using different solvers.

Code and data availability. The code used in this study is available on DTU Wind and Energy Systems' Gitlab (<https://gitlab.windenergy.dtu.dk/TOPFARM/PyWake>, DTU Wind Energy Systems, 2022a and <https://doi.org/10.5281/zenodo.6806136> Pedersen et al., 2023; <https://gitlab.windenergy.dtu.dk/TOPFARM/TopFarm2>, DTU Wind Energy Systems, 2022b and <https://doi.org/10.5281/zenodo.3553713>, Riva et al., 2019).

Author contributions. JCR prepared the first draft, devised the idea for the case study, contributed to the relaxation implementation in the code, led the numerical computations, and analyzed the results; RVR contributed to the literature review, methodology, and experiment design and was involved in the numerical computations; JQ contributed to the literature review, problem formulation, methodology, experiment design, and the drafting of the article;

MFM developed the methodology, implemented it in the software framework, and contributed to the problem formulation; MMP implemented smart-start and the automatic differentiation in the software and contributed to editing the article; PER contributed to the design experiment and the development of the methodology.

Competing interests. The contact author has declared that none of the authors has any competing interests.

Disclaimer. Publisher's note: Copernicus Publications remains neutral with regard to jurisdictional claims made in the text, published maps, institutional affiliations, or any other geographical representation in this paper. While Copernicus Publications makes every effort to include appropriate place names, the final responsibility lies with the authors.

Acknowledgements. The authors gratefully acknowledge the computational and data resources provided by the Sophia HPC cluster at the Technical University of Denmark, DOI: <https://doi.org/10.57940/FAFC-6M81> (Technical University of Denmark, 2019).

Financial support. This research has been supported by the Vestas.

Review statement. This paper was edited by Michael Muskulus and reviewed by Michael Muskulus and one anonymous referee.

References

- Afanasyeva, S., Saari, J., Pyrhönen, O., and Partanen, J.: Cuckoo search for wind farm optimization with auxiliary infrastructure, *Wind Energy*, 21, 855–875, 2018.
- Anaconda Software Distribution: <https://docs.anaconda.com/> (last access: November 2022), 2020.
- Bastankhah, M. and Porté-Agel, F.: A new analytical model for wind-turbine wakes, *Renew. Energ.*, 70, 116–123, <https://doi.org/10.1016/j.renene.2014.01.002>, 2014.
- Chen, L. and MacDonald, E.: A system-level cost-of-energy wind farm layout optimization with landowner modeling, *Energ. Convers. Manage.*, 77, 484–494, 2014.
- Ciavarra, A. W., Rodrigues, R. V., Dykes, K., and Réthoré, P.-E.: Wind farm optimization with multiple hub heights using gradient-based methods, *J. Phys. Conf. Ser.*, 2265, 022012, <https://doi.org/10.1088/1742-6596/2265/2/022012>, 2022.
- Dalla Longa, F., Kober, T., Badger, J., Volker, P., Hoyer-Klick, C., Hidalgo Gonzalez, I., Medarac, H., Nijs, W., Politis, S., Tarvydas, D., and Zucker, A.: Wind potentials for EU and neighbouring countries, Tech. rep., JRC Technical Report for the European Commission, <https://doi.org/10.2760/041705>, 2018.
- DTU Wind Energy Systems: PyWake, commit 3a61c8aec34a2505d0b460da2ad831aeaf46802b, <https://gitlab.windenergy.dtu.dk/TOPFARM/PyWake> (last access: November 2022), 2022a.
- DTU Wind Energy Systems: TOPFARM, commit c50abe91d08fe8ec81fc107e88c304f9a361d348, <https://gitlab.windenergy.dtu.dk/TOPFARM/TopFarm2> (last access: November 2022), 2022b.
- Feng, J., Shen, W. Z., and Li, Y.: An optimization framework for wind farm design in complex terrain, *Appl. Sci.-Basel*, 8, 2053, <https://doi.org/10.3390/app8112053>, 2018.
- Fischereit, J., Schaldemose Hansen, K., Larsén, X. G., van der Laan, M. P., Réthoré, P.-E., and Murcia Leon, J. P.: Comparing and validating intra-farm and farm-to-farm wakes across different mesoscale and high-resolution wake models, *Wind Energ. Sci.*, 7, 1069–1091, <https://doi.org/10.5194/wes-7-1069-2022>, 2022.
- Forsting, A. M., Rathmann, O. S., van der Laan, M., Trolborg, N., Gribben, B., Hawkes, G., and Branlard, E.: Verification of induction zone models for wind farm annual energy production estimation, *J. Phys. Conf. Ser.*, 1934, 012023, <https://doi.org/10.1088/1742-6596/1934/1/012023>, 2021.
- González, J. S., Trigo García, Á. L., Payán, M. B., Santos, J. R., and González Rodríguez, Á. G.: Optimal wind-turbine micro-siting of offshore wind farms: A grid-like layout approach, *Appl. Energ.*, 200, 28–38, <https://doi.org/10.1016/j.apenergy.2017.05.071>, 2017.
- Hou, P., Hu, W., Chen, C., Soltani, M., and Chen, Z.: Optimization of offshore wind farm layout in restricted zones, *Energy*, 113, 487–496, 2016.
- Kraft, D.: A Software Package for Sequential Quadratic Programming, Forschungsbericht, Wiss. Berichtswesen d. DFVLR, Deutsche Forschungs- und Versuchsanstalt für Luft- und Raumfahrt, Köln, <https://books.google.dk/books?id=4rKaGwAACAAJ> (last access: November 2022), 1988.
- Maclaurin, D., Duvenaud, D., and Adams, R. P.: Autograd: Effortless gradients in numpy, Wiss. Berichtswesen d. DFVLR, https://degenerateconic.com/uploads/2018/03/DFVLR_FB_88_28.pdf (last access: November 2022), 2015.
- Masoudi, S. M. and Baneshi, M.: Layout optimization of a wind farm considering grids of various resolutions, wake effect, and realistic wind speed and wind direction data: A techno-economic assessment, *Energy*, 244, 123188, <https://doi.org/10.1016/j.energy.2022.123188>, 2022.
- Mittal, P. and Mitra, K.: Determination of optimal layout of wind turbines inside a wind farm in presence of practical constraints, in: 2019 Fifth Indian Control Conference (ICC), 9–11 January 2019, New Delhi, India, <https://doi.org/10.1109/indiancc.2019.8715616>, 2019.
- Pedersen, M. M., van der Laan, P., Friis-Møller, M., Rinker, J., and Réthoré, P.-E.: DTUWindEnergy/PyWake: PyWake, Zenodo [code], <https://doi.org/10.5281/zenodo.2562662>, 2019.
- Pedersen, M. M., Larsen, G. C., and Ott, S.: Optimal open loop control of wind power plants, in: Abstract from Wind Energy Science Conference, 25 May 2021, Hanover, Germany, https://backend.orbit.dtu.dk/ws/portalfiles/portal/247826534/2021_WESC_Optimal_open_loop_control_of_wind_power_plants2.pdf (last access: 9 March 2024), 2021.
- Pedersen, M. M., van der Laan, P., Friis-Møller, M., Meyer Forsting, A., Riva, R., Alcayaga Román, L. A., Criado Risco, J., Quick, J., Schøler Christiansen, J. P., Olsen, B. T., Valotta Rodrigues, R.,

- and Réthoré, P.-E.: DTUWindEnergy/PyWake: PyWake (v2.5.0), Zenodo [code], <https://doi.org/10.5281/zenodo.6806136>, 2023.
- Perez-Moreno, S. S., Dykes, K., Merz, K. O., and Zaaier, M. B.: Multidisciplinary design analysis and optimisation of a reference offshore wind plant, *J. Phys.: Conf. Ser.*, 1037, 042004, <https://doi.org/10.1088/1742-6596/1037/4/042004>, 2018.
- Quick, J., Rethore, P.-E., Mølgaard Pedersen, M., Rodrigues, R. V., and Friis-Møller, M.: Stochastic gradient descent for wind farm optimization, *Wind Energ. Sci.*, 8, 1235–1250, <https://doi.org/10.5194/wes-8-1235-2023>, 2023.
- Reddy, S. R.: An efficient method for modeling terrain and complex terrain boundaries in constrained wind farm layout optimization, *Renew. Energ.*, 165, 162–173, <https://doi.org/10.1016/j.renene.2020.10.076>, 2021.
- Réthoré, P.-E., Fuglsang, P., Larsen, G. C., Buhl, T., Larsen, T. J., and Madsen, H. A.: TOPFARM: Multi-fidelity optimization of wind farms, *Wind Energy*, 17, 1797–1816, 2014.
- Riva, R., Liew, J. Y., Friis-Møller, M., Dimitrov, N. K., Barlas, E., Réthoré, P.-E., and Pedersen, M. M.: TopFarm2 (v2.2.0), Zenodo [code], <https://doi.org/10.5281/zenodo.3553713>, 2019.
- Riva, R., Liew, J., Friis-Møller, M., Dimitrov, N., Barlas, E., Réthoré, P.-E., and Beržonskis, A.: Wind farm layout optimization with load constraints using surrogate modelling, *J. Phys. Conf. Ser.*, 1618, 042035, <https://doi.org/10.1088/1742-6596/1618/4/042035>, 2020.
- Rodrigues, R. V., Friis-Møller, M., Dykes, K., Pollini, N., and Jensen, M.: A surrogate model of offshore wind farm annual energy production to support financial evaluation, *J. Phys. Conf. Ser.*, 2265, 022003, <https://doi.org/10.1088/1742-6596/2265/2/022003>, 2022.
- Shakoor, R., Hassan, M. Y., Raheem, A., and Rasheed, N.: Wind farm layout optimization using area dimensions and definite point selection techniques, *Renew. Energ.*, 88, 154–163, 2016.
- Sorkhabi, S. Y. D., Romero, D. A., Yan, G. K., Gu, M. D., Moran, J., Morgenroth, M., and Amon, C. H.: The impact of land use constraints in multi-objective energy-noise wind farm layout optimization, *Renew. Energ.*, 85, 359–370, <https://doi.org/10.1016/j.renene.2015.06.026>, 2016.
- Sorkhabi, S. Y. D., Romero, D. A., Beck, J. C., and Amon, C. H.: Constrained multi-objective wind farm layout optimization: Novel constraint handling approach based on constraint programming, *Renew. Energ.*, 126, 341–353, 2018.
- Tao, S., Xu, Q., Feijóo-Lorenzo, A. E., Zheng, G., and Zhou, J.: Optimal layout of a Co-Located wind/tidal current farm considering forbidden zones, *Energy*, 228, 120570, <https://doi.org/10.1016/j.energy.2021.120570>, 2021.
- Technical University of Denmark: Sophia HPC Cluster, <https://doi.org/10.57940/FAFC-6M81>, 2019.
- Valotta Rodrigues, R., Pedersen, M. M., Schøler, J. P., Quick, J., and Réthoré, P.-E.: Speeding up large-wind-farm layout optimization using gradients, parallelization, and a heuristic algorithm for the initial layout, *Wind Energ. Sci.*, 9, 321–341, <https://doi.org/10.5194/wes-9-321-2024>, 2024.
- Virtanen, P., Gommers, R., Oliphant, T. E., Haberland, M., Reddy, T., Cournapeau, D., Burovski, E., Peterson, P., Weckesser, W., Bright, J., van der Walt, S. J., Brett, M., Wilson, J., Millman, K. J., Mayorov, N., Nelson, A. R. J., Jones, E., Kern, R., Larson, E., Carey, C. J., Polat, İ., Feng, Y., Moore, E. W., VanderPlas, J., Laxalde, D., Perktold, J., Cimrman, R., Henriksen, I., Quintero, E. A., Harris, C. R., Archibald, A. M., Ribeiro, A. H., Pedregosa, F., van Mulbregt, P., and SciPy 1.0 Contributors: SciPy 1.0: Fundamental Algorithms for Scientific Computing in Python, *Nat. Methods*, 17, 261–272, <https://doi.org/10.1038/s41592-019-0686-2>, 2020.
- Wang, L., Tan, A. C., Gu, Y., and Yuan, J.: A new constraint handling method for wind farm layout optimization with lands owned by different owners, *Renew. Energ.*, 83, 151–161, 2015.